Theoretical and Experimental Analysis for the RMS Current Ripple Minimization in Induction Motor Drives Controlled by SVM Technique

Article *in* IEEE Transactions on Industrial Electronics · November 2004

DOI: 10.1109/TIE.2004.834967 · Source: IEEE Xplore

CITATIONS
86

READS
1,342

4 authors, including:

Giovanni Serra
University of Bologna
157 PUBLICATIONS **7,241** CITATIONS

SEE PROFILE

Luca Zarri
University of Bologna
173 PUBLICATIONS **4,236** CITATIONS

SEE PROFILE

Theoretical and Experimental Analysis for the RMS Current Ripple Minimization in Induction Motor Drives Controlled by SVM Technique

Domenico Casadei, *Associate Member, IEEE*, Giovanni Serra, *Associate Member, IEEE*, Angelo Tani, and Luca Zarri

***Abstract*—In this paper, an analytical approach useful for predicting the current ripple in induction motor drives controlled by space-vector modulation (SVM) technique is presented. The analysis is applied to determine the optimal modulation technique that minimizes the rms value of the current ripple. The minimization procedure is based on the analysis of the locus described by the current ripple in the α–β reference frame. As a result, a simple equation has been obtained, which allows the online calculation of the optimal SVM switching pattern. It has been verified that it is possible to obtain a current ripple lower than that of symmetric modulation, and with a reduced number of commutations. Experimental results are provided to confirm the theoretical approach.**

***Index Terms*—Harmonic distortion, induction motor drives, pulsewidth-modulated inverters.**

I. Introduction

THE wide diffusion of induction motor drives fed by voltage-source inverters (VSI) has encouraged considerable research activity concerning the performance of several modulation techniques, in terms of current ripple, optimized switching sequence, and increased voltage transfer ratio.

Many authors have shown that space-vector modulation (SVM) usually offers better performance compared to regular sampled carrier-based pulsewidth-modulation (PWM) technique [1]–[3].

It has been clearly documented in the literature that a suitable placement and sequence of the voltage space vectors within the cycle period can lead to lower current ripple and higher voltage transfer ratio, compared to regular sampled carrier-based PWM technique [4], [5].

Some authors have pointed out that the performance of the modulation strategies, in terms of current ripple, is defined by the placement of the zero-voltage space vectors within the cycle period [6], [7]. Several papers investigating optimal or suboptimal SVM techniques have been also published [8]–[10]. However, the approach utilized in this type of analysis is, in general, based on numerical simulations.

This paper addresses these issues by analyzing the relationship existing between the common-mode voltage and the placement of the zero-voltage space vectors, and by utilizing this degree of freedom to determine the optimal modulation technique in terms of rms value of the current ripple. In fact, a widely used method to evaluate the relative merits of different modulation techniques is to calculate the rms value of the load current ripple, which is strongly related to torque ripple and motor heating.

Manuscript received August 1, 2002; revised May 17, 2004. Abstract published on the Internet July 15, 2004. This paper was presented at the 2000 IEEE International Symposium on Industrial Electronics, Puebla, Mexico, Dec. 4–8.

The authors are with the Department of Electrical Engineering, University of Bologna, 40136 Bologna, Italy (e-mail: domenico.casadei@mail.ing.unibo.it).

Digital Object Identifier 10.1109/TIE.2004.834967

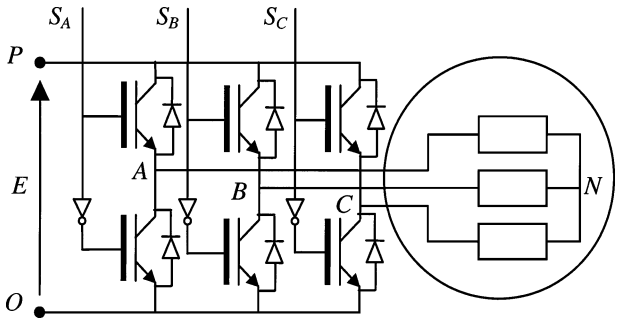

Fig. 1. Scheme of a PWM-VSI connected to a three-phase load.

In this paper, a method for calculating the analytical expression of the common-mode voltage that determines the minimum rms value of the load current ripple in each cycle period is presented. The results of the analysis consist of very simple equations, which can be used in digital control systems for online implementation of the optimal modulation technique.

The most important contribution of this study is the method proposed for the minimization of the rms value of the current ripple in induction motor drives. The optimal modulation technique should be considered as a result of the proposed method. It can be noted that using this technique it is possible to obtain a current ripple slightly lower than that of symmetric space vector modulation and with a reduced number of commutations for high values of the modulation index.

II. SVM

According to Fig. 1, in which a PWM inverter is supplying a three-phase load, the following equations can be written:

$$\begin{aligned} v_{AO} &= v_{AN} + v_{NO} \\ v_{BO} &= v_{BN} + v_{NO} \\ v_{CO} &= v_{CN} + v_{NO}. \end{aligned} \tag{1}$$

If s_A, s_B, and s_C are the switch states of the three inverter legs, and E is the dc-bus voltage, the inverter output voltages are

$$v_{AO} = s_A E \quad v_{BO} = s_B E \quad v_{CO} = s_C E. \tag{2}$$

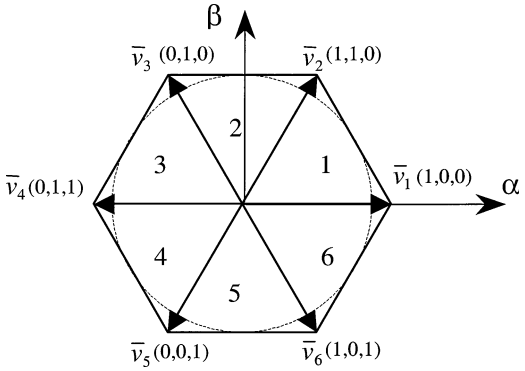

Fig. 2. Voltage vectors used in SVM technique, represented in α-β reference frame.

Introducing the space-vector representation in α–β reference frame, the following two fundamental equations can be determined:

$$\overline{v}_s = \frac{2}{3}E\left(s_A e^{j0} + s_B e^{j\frac{2\pi}{3}} + s_C e^{j\frac{4\pi}{3}}\right) \tag{3}$$

$$v_{NO} = \frac{s_A + s_B + s_C}{3}E. \tag{4}$$

The load voltage vector $\overline{v}_s$ and the common-mode voltage v_{NO} are completely defined once the three switch states s_A, s_B, and s_C are given.

As is known, there are eight possible combinations for s_A, s_B, and s_C in PWM inverters. Among these, six combinations determine the voltage space vectors represented in Fig. 2. Two combinations determine zero-voltage vectors.

Assuming that the desired voltage vector $\overline{v}_m$ lies in sector 1, the basic principle of SVM technique is to approximate $\overline{v}_m$ so that the average value of $\overline{v}_s$ in a given cycle period T_p is equal to $\overline{v}_m$, according to the following equation:

$$\overline{v}_m = \frac{1}{T_p}\int_0^{T_p} \overline{v}_s dt = \frac{2}{3}E\left(\delta_A e^{j0} + \delta_B e^{j\frac{2\pi}{3}} + \delta_C e^{j\frac{4\pi}{3}}\right) \tag{5}$$

where the duty cycles δ_A, δ_B, and δ_C are the average values of s_A, s_B, and s_C in a cycle period.

The average value of v_{NO} during the cycle period T_p is given by

$$V_{NO} = \frac{1}{T_p}\int_0^{T_p} v_{NO} dt = \frac{\delta_A + \delta_B + \delta_C}{3}E. \tag{6}$$

For given values of $\overline{v}_m$ and V_{NO}, the duty cycles δ_A, δ_B, and δ_C can be determined by the following inverse equations:

$$\delta_A = \frac{\overline{v}_m \cdot e^{j0} + V_{NO}}{E}$$

$$\delta_B = \frac{\overline{v}_m \cdot e^{j\frac{2\pi}{3}} + V_{NO}}{E}$$

$$\delta_C = \frac{\overline{v}_m \cdot e^{j\frac{4\pi}{3}} + V_{NO}}{E}. \tag{7}$$

These equations show that, for a given value of $\overline{v}_m$, there are infinite possible solutions for the duty cycles. The common-mode voltage V_{NO} represents a degree of freedom, which can be utilized to define different modulation techniques, characterized by different current ripple and maximum inverter output voltage.

TABLE I
MAXIMUM INVERTER OUTPUT VOLTAGE FOR DIFFERENT VALUES OF V_{NO}

Modulation technique	V_{NO}	V_{max}
Sinusoidal PWM	$\frac{E}{2}$	$\frac{E}{2}$
Two phase modulation (a)	V_{NOmin}	$\frac{E}{\sqrt{3}}$
Two phase modulation (b)	V_{NOmax}	$\frac{E}{\sqrt{3}}$
Symmetric modulation	$\frac{V_{NOmin} + V_{NOmax}}{2}$	$\frac{E}{\sqrt{3}}$

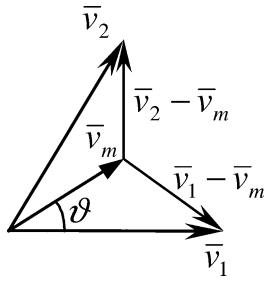

Fig. 3. Representation of the voltage vectors affecting the current ripple locus when the reference voltage $\overline{v}_m$ is in sector 1.

The duty cycles must satisfy the following constraint:

$$\delta_A, \delta_B, \delta_C \in [0, 1]. \tag{8}$$

Combining (7) and (8) yields the range of variation for V_{NO}

$$V_{NO} > V_{NOmin} = -min\left\{\overline{v}_m \cdot e^{j0}, \overline{v}_m \cdot e^{j\frac{2\pi}{3}}, \overline{v}_m \cdot e^{j\frac{4\pi}{3}}\right\} \tag{9}$$

$$V_{NO} < V_{NO\max} = E - \max\left\{\overline{v}_m \cdot e^{j0}, \overline{v}_m \cdot e^{j\frac{2\pi}{3}}, \overline{v}_m \cdot e^{j\frac{4\pi}{3}}\right\}. \tag{10}$$

As an example, Table I shows V_{NO} and the maximum inverter output voltage ($V_{\max}$) for the most common modulation techniques, which are sinusoidal PWM, two-phase modulation, and symmetric modulation [5].

III. EFFECTS OF THE ZERO SEQUENCE

Assuming that the desired voltage vector $\overline{v}_m$ lies in sector 1 (Fig. 3), the general SVM switching pattern represented in Fig. 4 can be utilized to approximate $\overline{v}_m$ in the cycle period T_p. The voltage vector sequence ensures that only one inverter leg commutates at each voltage vector change.

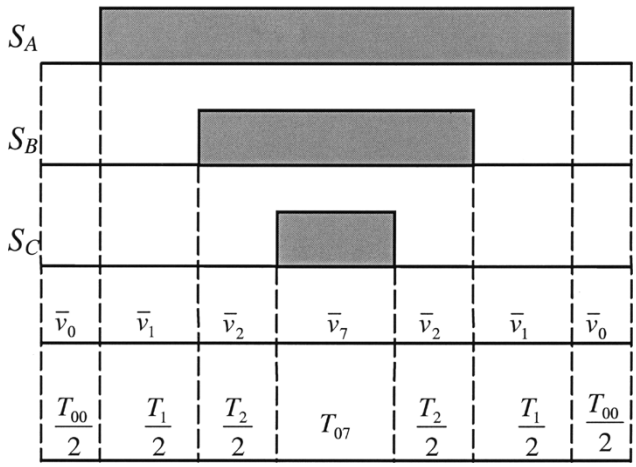

Fig. 4. General SVM switching pattern for a reference voltage vector lying in sector 1.

With reference to Fig. 4, the following time intervals can be defined:

T_{00} time interval of application of $\overline{v}_0$;
T_{07} time interval of application of $\overline{v}_7$;
T_0 $= T_{00} + T_{07}$ total time interval of application of zero-voltage vectors;
T_1 $= T_A - T_B$ time interval of application of $\overline{v}_1$;
T_2 $= T_B - T_C$ time interval of application of $\overline{v}_2$.

For the feasibility of the modulation technique, T_1, T_2, and T_0 must satisfy the following equation:

$$T_0 + T_1 + T_2 = T_p. \tag{11}$$

The duty cycles related to these time intervals are given by

$$\delta_1 = \frac{T_1}{T_p} \quad \delta_2 = \frac{T_2}{T_p} \quad \delta_0 = \frac{T_0}{T_p}. \tag{12}$$

Taking (7) into account, (12) can be expressed as follows:

$$\delta_1 = \delta_A - \delta_B = -\frac{\sqrt{3}\overline{v}_m \cdot e^{j\frac{\pi}{6}}}{E} \tag{13}$$

$$\delta_2 = \delta_B - \delta_C = \frac{\sqrt{3}\overline{v}_m \cdot e^{j\frac{\pi}{2}}}{E} \tag{14}$$

$$\delta_0 = 1 - \delta_1 - \delta_2. \tag{15}$$

These equations show that δ_1, δ_2, δ_0, and then T_1, T_2, and T_0 are not affected by the value of V_{NO}. As a consequence, the choice of V_{NO} can only determine how the total time of application of the zero-voltage vector is distributed between the time intervals T_{00} and T_{07}.

When the required voltage vector $\overline{v}_m$ is applied to the motor, the current $\overline{i}_{sm}$ is flowing in the stator winding. The actual value of the stator voltage $\overline{v}_s$ differs from $\overline{v}_m$ because $\overline{v}_s$ can assume only a finite number of configurations (Fig. 2). It is then possible to define the voltage and the current ripple vectors as follows:

$$\overline{v}_{\rm rip} = \overline{v}_s - \overline{v}_m \tag{16}$$

$$\overline{i}_{\rm rip} = \overline{i}_s - \overline{i}_{sm} \tag{17}$$

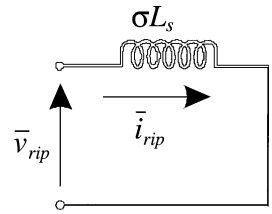

Fig. 5. Simplified circuit of the induction motor valid for small current variations.

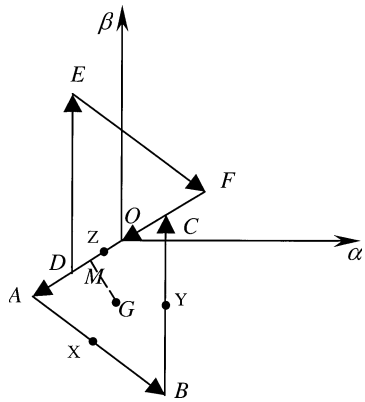

Fig. 6. Locus described by the current ripple vector in the α–β reference frame.

where $\overline{i}_s$ is the actual value of the stator current vector.

Taking into account the principle operation of SVM technique, the mean value of $\overline{v}_{\rm rip}$ during a cycle period T_p is zero.

The relation between $\overline{v}_{\rm rip}$ and $\overline{i}_{\rm rip}$ can be determined by the simplified linear circuit of Fig. 5, yielding

$$\frac{d\overline{i}_{\rm rip}}{dt} = \frac{(\overline{v}_s - \overline{v}_m)}{\sigma L_s}. \tag{18}$$

Also, the current ripple has zero mean value in a cycle period. Taking (18) into account, it is possible to determine the locus described in the $\alpha - \beta$ reference frame by the vector $\overline{i}_{\rm rip}$ during T_p. Fig. 6 shows the locus obtained with reference to the SVM switching pattern of Fig. 4.

The vectors $\overline{AO}$, $\overline{BA}$, $\overline{CB}$, and $\overline{OC}$ represent the variations of the current ripple determined, respectively, by the application of $\overline{v}_0$, $\overline{v}_1$, $\overline{v}_2$, and $\overline{v}_7$ in the first half of the cycle period. These vectors are given by

$$\overline{AO} = -\frac{T_{00}}{2\sigma L_s}\overline{v}_m \tag{19}$$

$$\overline{BA} = \frac{T_1}{2\sigma L_s}(\overline{v}_1 - \overline{v}_m) \tag{20}$$

$$\overline{CB} = \frac{T_2}{2\sigma L_s}(\overline{v}_2 - \overline{v}_m) \tag{21}$$

$$\overline{OC} = -\frac{T_{07}}{2\sigma L_s}\overline{v}_m. \tag{22}$$

The current ripple locus shown in Fig. 6 (triangle ABC) has been drawn taking Fig. 3 into account, where the vectors $\overline{v}_m$, $\overline{v}_1 - \overline{v}_m$, and $\overline{v}_2 - \overline{v}_m$ are represented.

Adding (19) to (22), it is possible to determine the vector $\overline{AC}$ as follows:

$$\overline{AC} = \overline{AO} + \overline{OC} = -\frac{T_0}{2\sigma L_s}\overline{v}_m. \tag{23}$$

The vector $\overline{AC}$ represents the total current ripple variation due to the application of zero-voltage vectors. According to the previous equations, the length of vectors $\overline{BA}$, $\overline{CB}$, and $\overline{AC}$ does not depend on the common-mode voltage. In fact, it has been already verified that V_{NO} does not affect T_1, T_2, and T_0. Therefore, the shape of the triangle ABC is completely defined by $\overline{v}_m$. A similar analysis can be carried out for the triangle DEF, which represents the locus described by the current ripple during the second half of the cycle period.

From Fig. 6 it appears that it is possible to modify the relative position between the two triangles by changing the ratio between $\overline{AO}$ and $\overline{OC}$. Since the amplitude of these two vectors is proportional to T_{00} and T_{07} respectively, the relative position of the two triangles can be modified by changing the value of V_{NO}. As a consequence, each modulation strategy, which is defined by a given value of V_{NO}, is characterized by a different current ripple locus.

IV. Optimal Modulation Technique

The parameter that is commonly used to represent the distortion of a waveform is the rms value of the variation, defined as

$$I_{\mathrm{ripRMS}} = \sqrt{i^2_{\mathrm{ripRMS}A} + i^2_{\mathrm{ripRMS}B} + i^2_{\mathrm{ripRMS}C}}. \tag{24}$$

As the locus described by $\overline{i}_{\mathrm{rip}}$ is symmetrical with respect to the origin of the reference frame, the rms value of the current ripple can be expressed as

$$I_{\mathrm{ripRMS}} = \sqrt{\frac{3}{2}}\sqrt{\frac{2}{T_p}\int_0^{\frac{T_p}{2}} i^2_{\mathrm{rip}}dt}. \tag{25}$$

In (25), i_{rip} represents the magnitude of $\overline{i}_{\mathrm{rip}}$. In order to determine the operating conditions that minimize the current ripple, a geometrical analysis of the locus described in the α–β reference frame is necessary. Owing to the symmetry, the analysis can be focused only on the triangle ABC, which is described in the first half of the cycle period.

As a first step, it is interesting to determine the average value of the current ripple vector in $T_p/2$

$$\begin{aligned}\overline{i}_{\mathrm{ripmean}} &= \frac{2}{T_p}\int_0^{\frac{T_p}{2}} \overline{i}_{\mathrm{rip}}dt \\ &= \frac{2}{T_p}\left[\int_0^{\frac{T_{00}}{2}} \overline{i}_{\mathrm{rip}}dt + \int_{\frac{T_{00}}{2}}^{\frac{T_{00}+T_1}{2}} \overline{i}_{\mathrm{rip}}dt \right. \\ &\quad \left. + \int_{\frac{T_{00}+T_1}{2}}^{\frac{T_{00}+T_1+T_2}{2}} \overline{i}_{\mathrm{rip}}dt + \int_{\frac{T_p-T_{07}}{2}}^{\frac{T_p}{2}} \overline{i}_{\mathrm{rip}}dt\right].\end{aligned} \tag{26}$$

By developing (26), and by geometrical considerations on Fig. 6, the following equation can be derived:

$$\overline{i}_{\mathrm{ripmean}} = \frac{T_1}{T_p}\overline{\mathrm{XO}} + \frac{T_2}{T_p}\overline{\mathrm{YO}} + \frac{T_0}{T_p}\overline{\mathrm{ZO}} = \overline{GO} \tag{27}$$

where X, Y, and Z are the middle point of the triangle sides (triangle ABC in Fig. 6).

It is possible to verify that (27) is similar to the equation used to calculate the center of mass of the triangle ABC with respect to point O. As in mechanics, the position of the center of mass (point G) can be defined with reference to any other point P lying in α–β reference frame, simply substituting O with P in (27). So, the position of the point G with respect to points A, B, and C does not depend on the reference frame and, therefore, neither on V_{NO}. It is then opportune to refer $\overline{i}_{\mathrm{rip}}$ to this point. Introducing an auxiliary vector $\overline{i}'$, the current ripple can be expressed as follows:

$$\overline{i}_{\mathrm{rip}} = \overline{GO} + \overline{i}'. \tag{28}$$

It is possible to verify that averaging (28), $\overline{GO}$ being the average value of $\overline{i}_{\mathrm{rip}}$, leads to the conclusion that the average value of $\overline{i}'$ in the time interval $T_p/2$ is zero.

Substituting (28) in (25), and taking the previous consideration into account, yields

$$\begin{aligned}\sqrt{\frac{2}{3}}I_{\mathrm{ripRMS}} &= \sqrt{\frac{2}{T_p}\int_0^{\frac{T_p}{2}} |\overline{GO} + \overline{i}'|^2 dt} \\ &= \sqrt{\frac{2}{T_p}\int_0^{\frac{T_p}{2}} i'^2 dt + GO^2}.\end{aligned} \tag{29}$$

In (29), $\int_0^{T_p/2} i'^2 dt$ does not depend on V_{NO}, therefore, the rms value of the current ripple is minimized when the vector $\overline{GO}$ has the minimum length. This condition is achieved when the point M, which represents the projection of G on $\overline{AC}$, coincides with point O.

For the application of this basic principle it is useful to introduce the parameter λ, representing the duty cycle of $\overline{v}_0$ with respect to the total time interval of application of zero-voltage vectors T_0

$$\lambda = \frac{T_{00}}{T_0}. \tag{30}$$

Using the previous geometrical considerations, and after some analytical developments given in the Appendix, leads to the following equation:

$$\lambda = \frac{1}{2} + \frac{\delta_1\delta_2(\delta_1 - \delta_2)}{3\rho^2\delta_0} \tag{31}$$

where ρ is the modulation index defined as

$$\rho = \frac{v_m}{\frac{E}{\sqrt{3}}}. \tag{32}$$

Equation (31) is the final equation, which allows the determination of the switching pattern for the optimum modulation technique in each cycle period. Once $\overline{v}_m$ is known, it is possible

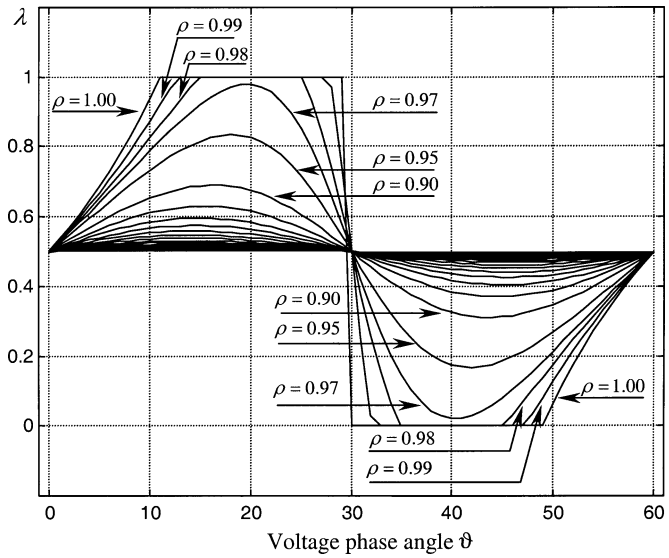

Fig. 7. Behavior of λ as function of ϑ with the modulation index ρ as a parameter.

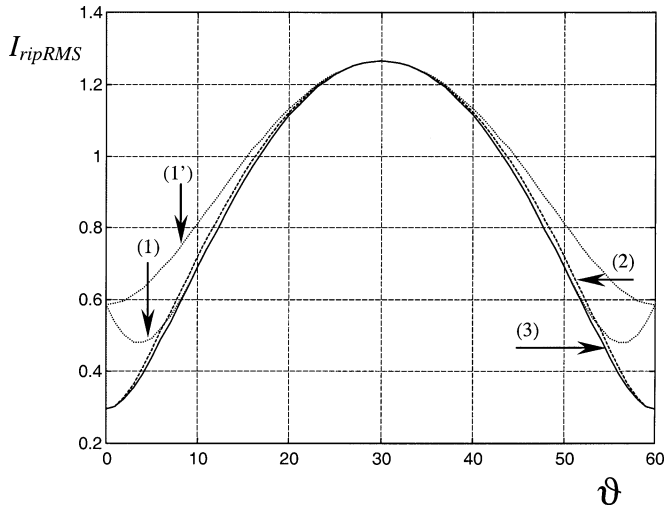

Fig. 8. RMS value of the current ripple in a cycle period as a function of ϑ, for $\rho = 1$. (1), (1′) Two-phase modulation type (a) and (b). (2) Symmetric modulation. (3) Optimal modulation.

to calculate δ_1, δ_2, and δ_0 by using (13)–(15), and to calculate ρ by using (32). Then, introducing the value of λ calculated by (31) in (30) gives T_{00}, which represents the time interval of application of $\overline{v}_0$. The time intervals T_1, T_2, and T_0 can be calculated by (12).

Finally, the time interval of application of $\overline{v}_7$ can be calculated by $T_{07} = T_0 - T_{00}$. In this way, all the time intervals necessary for a digital implementation of the optimum modulation algorithm are known. In case of analog implementation, the common-mode voltage V_{NO} should be calculated as a function of λ in order to solve (7). For this purpose, using (12)–(15) and (30), the following relationships can be determined:

$$\begin{aligned}\delta_A &= \delta_1 + \delta_2 + \delta_C \\ \delta_B &= \delta_2 + \delta_C \\ \delta_C &= (1-\lambda)\delta_0. \end{aligned} \tag{33}$$

Substituting (33) in (6) yields

$$\frac{V_{NO}}{E} = \frac{1}{2} + \left(\frac{1}{2} - \lambda\right)\delta_0 + \frac{\delta_2 - \delta_1}{6}. \tag{34}$$

This equation allows the determination of the common-mode voltage V_{NO}, once the duty-cycles δ_0, δ_1, δ_2, and λ are known.

Fig. 7 shows the behavior of λ (duty cycle of $\overline{v}_0$) as a function of ϑ (phase angle of the voltage vector $\overline{v}_m$), assuming the modulation index ρ as a parameter. For high values of ρ the duty cycle of $\overline{v}_0$ is close to 1, i.e., $\overline{v}_0$ is applied for most of the total time interval of application of zero-voltage vectors. This means that the optimal modulation technique has a behavior similar to that of the two-phase modulation technique.

When ϑ is lower than 30°, λ assumes values higher than 0.5, i.e., the zero-voltage vector is approximated using mainly $\overline{v}_0$. On the contrary, when ϑ is higher than 30°, λ assumes values lower than 0.5, i.e., the zero-voltage vector is approximated using mainly $\overline{v}_7$.

V. Numerical Simulations

In order to verify the performance of the optimal modulation strategy in terms of current ripple, some numerical simulations have been performed with reference to an induction motor having the following parameters:

$$\begin{aligned} R_s &= 0.42\ \Omega \\ R_r &= 0.31\ \Omega \\ L_s &= L_r = 50.51\ \text{mH} \\ M &= 49.04\ \text{mH}. \end{aligned}$$

The dc-bus voltage is 311 V and the cycle period T_p is 200 μs. The rms value of the current ripple has been calculated using (25).

Fig. 8 compares the results obtained by three modulation techniques, namely, two-phase modulation, symmetric modulation, and optimal modulation. In Fig. 8, ϑ varies from 0° to 60°, and $\rho = 1$. When ϑ is around 30°, the performance of the three modulation techniques is quite similar, whereas for ϑ close to 0° and 60°, symmetric and optimal modulation techniques perform better than two-phase modulation technique.

Fig. 9 illustrates the results obtained for $\rho = 0.8$. In this case, the numerical simulations have been carried out for the sinusoidal PWM technique, also. For $\rho = 0.8$ the difference between optimal and symmetric modulations, and the other modulation types is more evident than for $\rho = 1$.

Fig. 10 shows the rms value of the current ripple, calculated over a fundamental period, as a function of ρ. It can be noted that the behavior of the symmetric modulation in terms of current ripple is similar to that of the optimal modulation for any value of ρ. However, the optimal modulation is superior to symmetric modulation, in terms of switching frequency, for high values of ρ. In fact, in these operating conditions the optimal modulation performs like the two-phase modulation, which is characterized by a switching frequency lower than that of symmetric modulation.

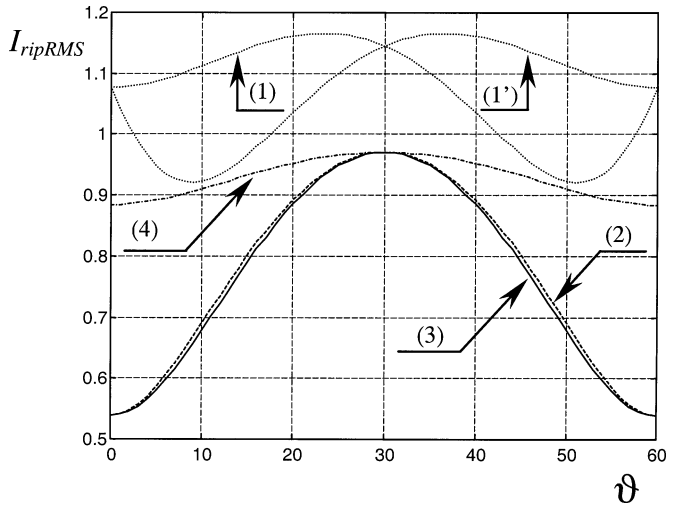

Fig. 9. RMS value of the current ripple in a cycle period as a function of ϑ, for $\rho = 0.8$. (1), (1′) Two-phase modulation type (a) and (b). (2) Symmetric modulation. (3) Optimal modulation. (4) Sinusoidal PWM.

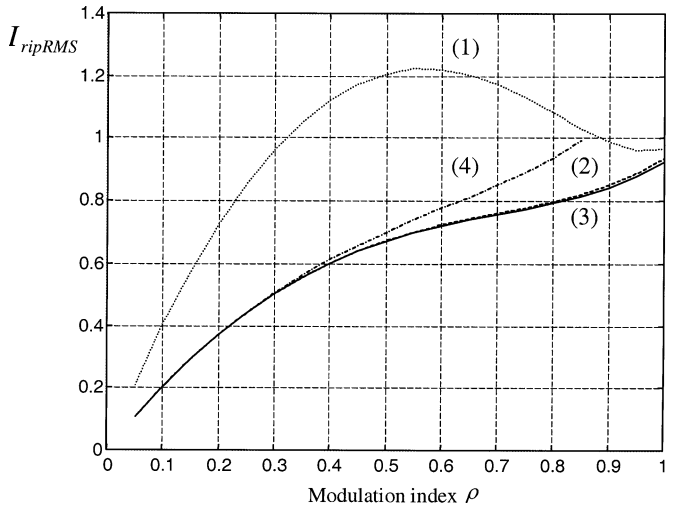

Fig. 10. RMS value of the current ripple in a fundamental period as a function of ρ. (1) Two-phase modulation type (a) and (b). (2) Symmetric modulation. (3) Optimal modulation. (4) Sinusoidal PWM.

This is confirmed in Fig. 11, where the switching frequency, expressed in per unit (p.u.) of the sinusoidal PWM switching frequency, is plotted as a function of ρ for the different types of modulation.

The results illustrated in Fig. 10 allow an effective comparison among different types of modulation techniques in terms of current ripple. The rms value of the current ripple has been widely utilized in several papers dealing with SVM techniques [1], [4], [7], [8]. In some of these papers, analytical relationships or diagrams have been proposed for the calculation of the rms value of the current ripple for given operating conditions. The validity of these results has also been investigated with experimental tests [1], [8]. The application of these relationships, with the same parameter values utilized in this section, yields numerical values that are in good agreement with those shown in Fig. 10.

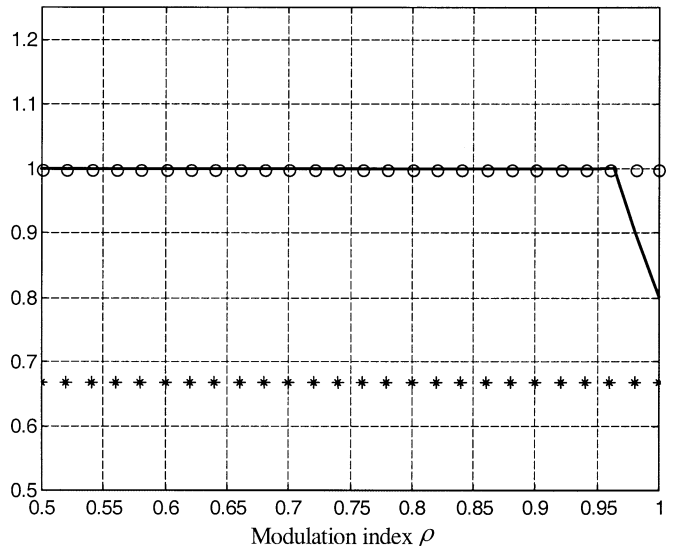

Fig. 11. Switching frequency in p.u. of the sinusoidal PWM switching frequency as a function of ρ. *: Two-phase modulation, °: Sinusoidal PWM, symmetric modulation. ——: Optimal modulation.

VI. Experimental Results

In order to confirm the theoretical approach, a complete drive system has been developed in the laboratory. The experimental setup consists of an insulated gate bipolar transistor (IGBT) inverter, a TMS320F2407 digital signal processor (DSP), and a four-pole squirrel-cage induction motor, characterized by the following rated data:

$$P = 4 \text{ kW}$$
$$n = 1425 \text{ r/min}$$
$$V = 220 \text{ V}$$
$$f = 50 \text{ Hz}$$
$$I = 16 \text{ A}.$$

The induction motor is controlled according to the well-known constant V/Hz operation and the cycle period T_p has been chosen equal to 200 μs. The program implemented on the DSP can switch instantaneously from a modulation strategy to another one, thus allowing the comparison among different modulation strategies to be carried out in the same operating conditions.

Fig. 12 shows the current ripple behavior with $\rho = 0.6$, for the two-phase modulation [Fig. 12(a)], the symmetric modulation [Fig. 12(b)], and the optimal modulation [Fig. 12(c)]. According to the theoretical results presented in the previous sections, the two-phase modulation clearly shows the highest ripple, whereas optimal and symmetric modulations show comparable results.

Fig. 13 illustrates with more detail the current ripple in the same operating conditions as in Fig. 12. In Fig. 13, the correlation between the applied voltage vectors and the corresponding current variations is also emphasized.

Fig. 14 shows the current ripple behavior with $\rho = 1$. In this case, the improvement of both symmetric and optimal modulation techniques in terms of current ripple is negligible with respect to the two-phase modulation. However, the optimal mod-

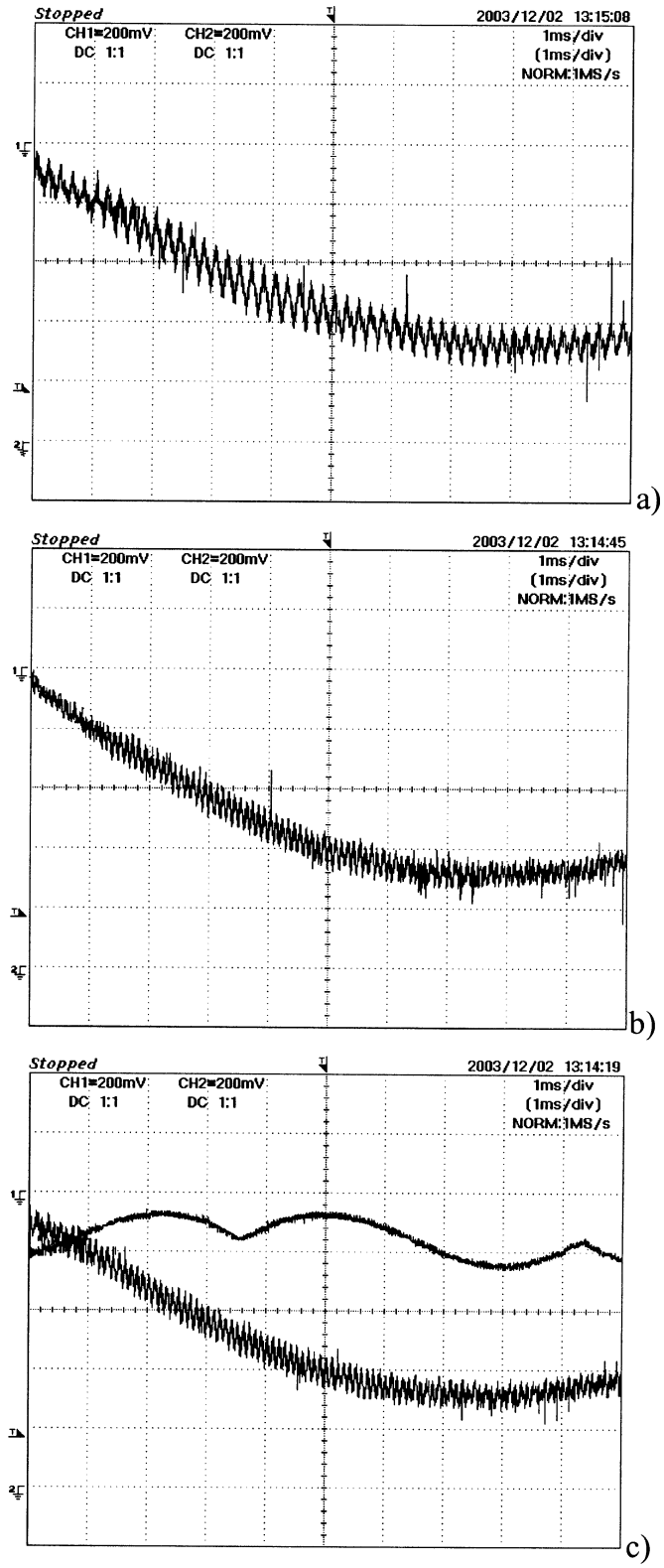

Fig. 12. Current ripple behavior with $\rho = 0.6$. (a) Two-phase modulation. (b) Symmetric modulation. (c) Optimal modulation, with the corresponding $\lambda(t)$ waveform.

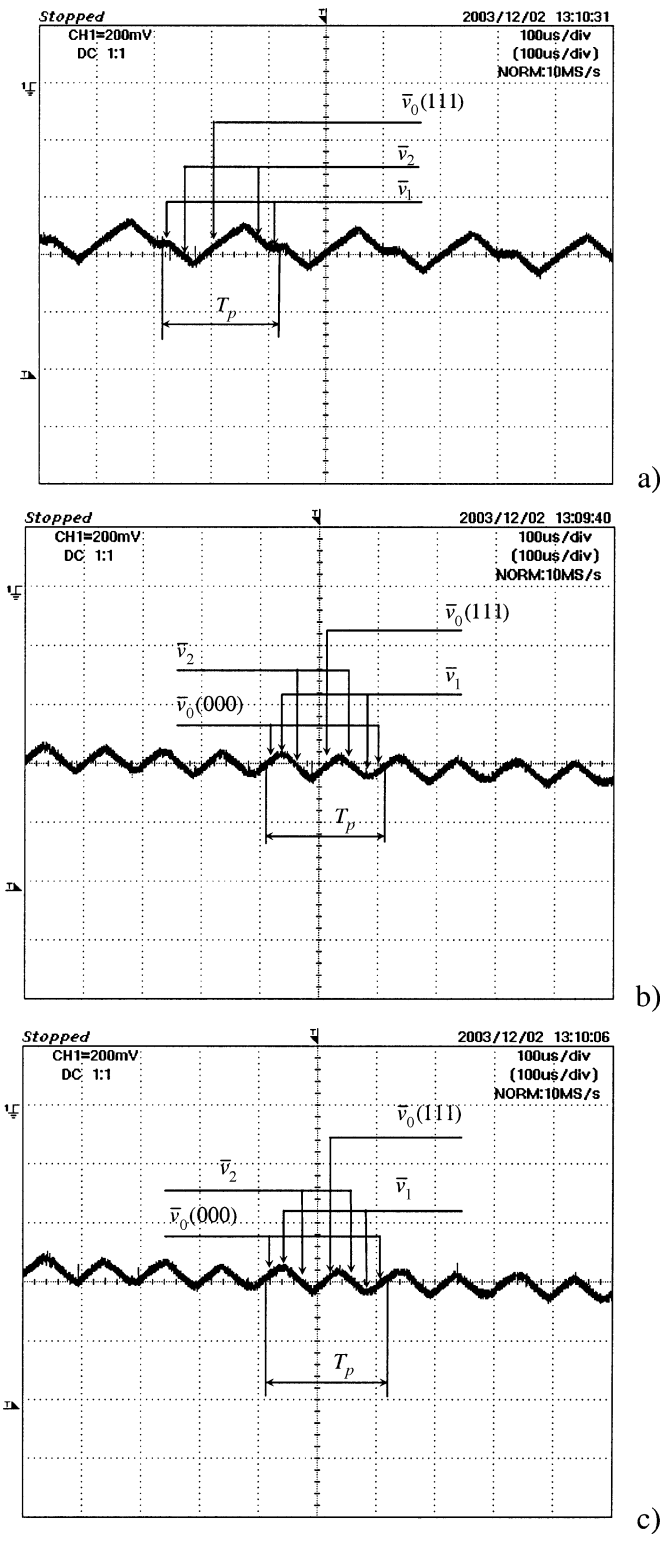

Fig. 13. Details of the current ripple with $\rho = 0.6$. (a) Two-phase modulation. (b) Symmetric modulation. (c) Optimal modulation.

ulation technique should be preferred to the symmetric modulation one owing to the lower switching frequency. This can be verified analyzing Fig. 15, where the current ripple in the same operating conditions is clearly emphasized. As can be seen, the optimal strategy uses only one type of zero vector (000), placed at the beginning and at the end of the cycle period, determining a reduction of the switching frequency with respect to the symmetric modulation.

The two-phase modulation uses only one type of zero vector (111), placed in the middle of the cycle period, determining the

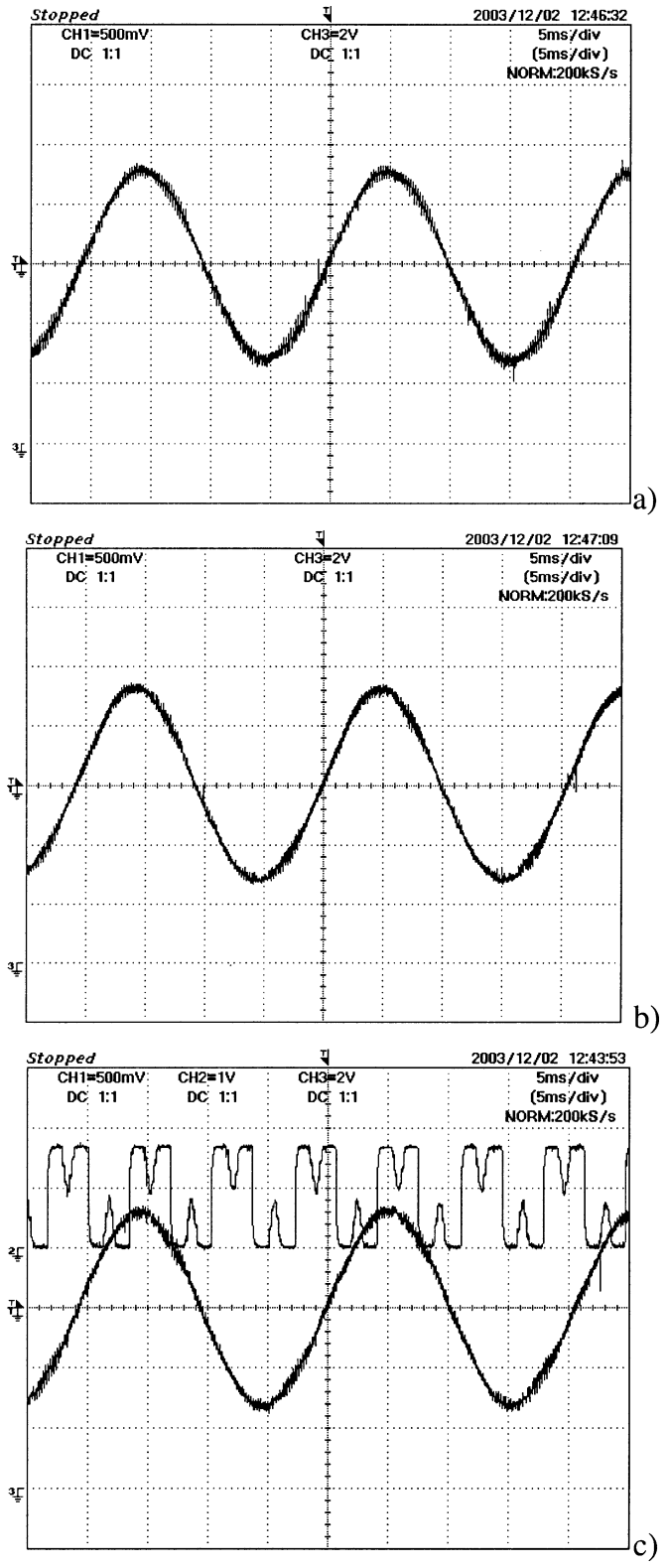

Fig. 14. Current waveforms with $\rho = 1$. (a) Two-phase modulation. (b) Symmetric modulation. (c) Optimal modulation, with the corresponding $\lambda(t)$ waveform.

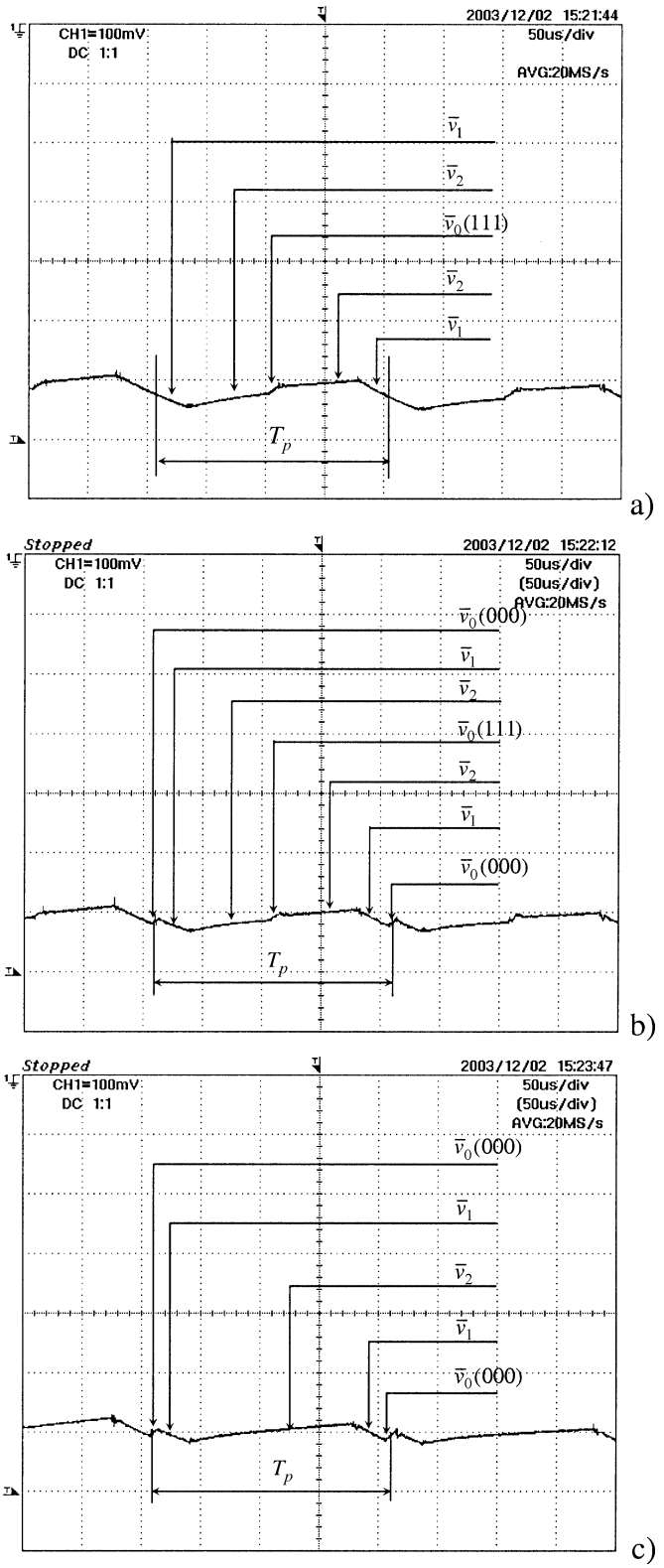

Fig. 15. Details of the current ripple with $\rho = 1$. (a) Two-phase modulation. (b) Symmetric modulation. (c) Optimal modulation.

same number of switch commutations as in the case of optimal modulation, but producing a higher peak-to-peak current ripple.

Finally, Fig. 16 shows three waveforms representing the time behavior of the switch commutations number in a fundamental period, for two-phase modulation [*(a)* in the figure], symmetric modulation [*(b)* in the figure], and optimal modulation [*(c)* in the figure]. As can be seen, the optimal modulation is characterized by a number of commutations that comes between those of symmetric modulation and two-phase modulation.

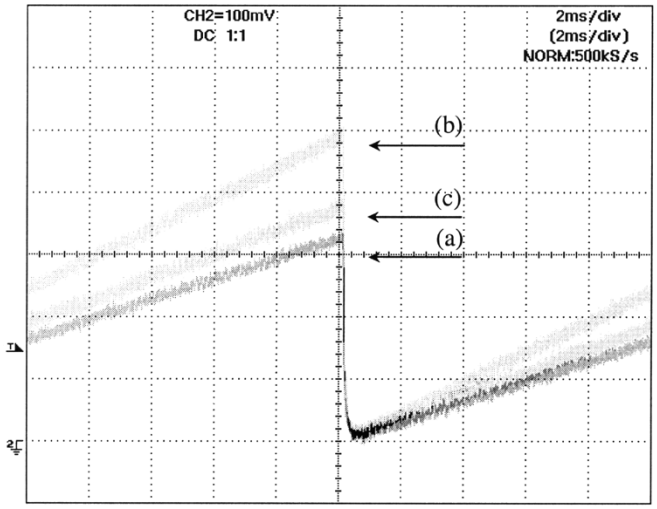

Fig. 16. Waveforms representing the switch commutations number in a fundamental period with $\rho = 1$. (a) Two-phase modulation. (b) Symmetric modulation. (c) Optimal modulation.

VII. Conclusion

An analytical approach for the analysis of current ripple in SVM-controlled induction motor drives has been presented. The main feature is the general validity, which makes it possible to employ this approach for determining the characteristics of any type of modulation technique.

In this paper, the proposed method has been applied to define the optimal SVM technique, characterized by the minimum rms value of the current ripple calculated in the cycle period and, as a consequence, over the fundamental period.

Analyzing the geometrical properties of the locus described by the current ripple, a simple equation has been determined, which allows the calculation of the duty cycles of the two types of zero-voltage vectors and then the determination of the switching pattern of the optimal SVM technique.

The performance of the optimal modulation technique has been compared with that of the most commonly used modulation techniques, namely, sinusoidal PWM, two-phase modulation, and symmetric modulation.

The results obtained show that the optimal modulation performs better than two-phase modulation and sinusoidal modulation in terms of current ripple. The comparison with symmetric modulation shows quite similar performance. Actually, the current ripple for the optimal SVM technique is slightly lower than that of symmetric modulation. The main difference between the two modulation techniques is that the optimal modulation shows lower switching frequencies for high values of the modulation index.

Experimental tests have been performed, emphasizing the behavior of the different modulation strategies and confirming the results predicted by the theoretical approach.

Appendix

The determination of (31) will be outlined in this appendix with reference to the case considered in Fig. 6.

Firstly, it is worth noting that the parameter λ defined in (30) can be expressed as the ratio between the lengths of the segments $\overline{MA}$ and $\overline{CA}$, proportional to T_{00} and T_0, respectively, as follows:

$$\lambda = \frac{MA}{CA}. \tag{A1}$$

As M is the projection of G on $\overline{CA}$, the length of the segment $\overline{MA}$ can be found as follows:

$$MA = \overline{GA} \cdot \frac{\overline{v}_m}{|\overline{v}_m|}. \tag{A2}$$

Substituting (A2) in (A1) leads to

$$\lambda = \frac{\overline{GA}}{CA} \cdot \frac{\overline{v}_m}{|\overline{v}_m|}. \tag{A3}$$

In order to determine an explicit expression for $\overline{GA}$, (27) must be written in a more general form, as follows:

$$\overline{GO} = \frac{T_1}{T_p}\frac{\overline{AO}+\overline{BO}}{2} + \frac{T_2}{T_p}\frac{\overline{BO}+\overline{CO}}{2} + \frac{T_3}{T_p}\frac{\overline{CO}+\overline{AO}}{2}. \tag{A4}$$

As the position of G does not depend on the origin O of the reference frame, the point G can be determined with respect to the vertex A by substituting O with A in (A4). After some manipulations it is possible to obtain the following relationship:

$$\overline{GA} = \frac{T_1+T_2}{2T_p}\overline{BA} + \frac{T_0+T_2}{2T_p}\overline{CA}. \tag{A5}$$

Taking (32) into account, a new formulation of the duty-cycle expressions (13) and (14) can be determined, leading to

$$\delta_1 = \rho\cos\left(\vartheta + \frac{\pi}{6}\right) \tag{A6}$$

$$\delta_2 = \rho\sin(\vartheta) \tag{A7}$$

where ϑ is the phase angle of the reference voltage vector $\overline{v}_m$.

By mean of (A5)–(A7), (20), (23), and (15), the following expression for λ can be determined:

$$\lambda = \frac{1}{2}(1-\delta_0)\left(\frac{2}{\sqrt{3}}\frac{\cos\vartheta}{\rho} - 1\right)\frac{\delta_1}{\delta_0} + \frac{1}{2}(1-\delta_1). \tag{A8}$$

Instead of (A8), a more compact expression of λ, useful for the implementation on a low-cost fixed-point DSP, can be determined. For this purpose, from (A6) and (A7) it is possible to obtain the following equations:

$$\cos\vartheta = \frac{1}{\sqrt{3}}\frac{2\delta_1+\delta_2}{\rho} \tag{A9}$$

$$\sin\vartheta = \frac{\delta_2}{\rho}. \tag{A10}$$

Being that $\cos^2\vartheta + \sin^2\vartheta = 1$, (A9) and (A10) lead to

$$\delta_1^2 + \delta_2^2 + \delta_1\delta_2 = \frac{3}{4}\rho^2. \tag{A11}$$

Substituting (A9) in (A8) and taking into account (15) and (A11), after some tedious manipulations, (31) can be finally determined.

References

[1] W. van der Broeck and H. C. Skudenly, "Analysis and realization of a pulsewidth modulator based on voltage space vectors," *IEEE Trans. Ind. Applicat.*, vol. 24, pp. 142–150, Jan./Feb. 1988.

[2] H. W. van der Broeck, "Analysis of the harmonics in voltage fed inverter drives caused by PWM schemes with discontinuous switching operation," in *Proc. EPE*, Florence, Italy, 1991, pp. 3261–3266.
[3] J. Holtz, "Pulsewidth modulation—A survey," *IEEE Trans. Ind. Electron.*, vol. 39, pp. 410–420, Oct. 1992.
[4] S. Fukuda and K. Suzuki, "Harmonic evaluation of two-level carrier-based PWM methods," in *Proc. EPE*, vol. 2, 1997, pp. 2331–2336.
[5] D. Casadei, G. Serra, A. Tani, and L. Zarri, "Analysis of the current ripple in induction motor drives controlled by SVM technique," in *Proc. EPE*, Lausanne, Switzerland, 1999, CD-ROM.
[6] L. Abrahm and R. Blümel, "Optimization of three phase pulse pattern by variable zero sequence component," in *Proc. EPE*, vol. 3, Florence, Italy, 1991, pp. 272–277.
[7] F. Jenni and D. Wueest, "The optimization parameters of space vector modulation," in *Proc. EPE*, Brighton, U.K., 1993, pp. 376–381.
[8] V. R. Stefanovic and S. N. Vukosavic, "Space vector PWM voltage control with optimized switching strategy," in *Conf. Rec. IEEE-IAS Annu. Meeting*, vol. 1, 1992, pp. 1025–1033.
[9] S. V. Shevtsov, D. Izosimov, and S. E. Ryvkin, "Space vector based simplex pulse-width modulation methods of 3-phase VSI control," in *Proc. IEEE IECON'94*, vol. 1, Bologna, Italy, 1994, pp. 520–525.
[10] D. G. Holmes, "The significance of zero space vector placement for carrier based PWM schemes," *IEEE Trans. Ind. Applicat.*, vol. 32, pp. 1122–1129, Sept./Oct. 1996.

Domenico Casadei (A'01) received the "Laurea" degree, with honors, in electrical engineering from the University of Bologna, Bologna, Italy, in 1974.

He joined the Electrical Engineering Department, University of Bologna, in 1975. He is currently Professor of Electrical Drives. His scientific work is related to electrical machines and drives, linear motors, and power electronics. He has published extensively in technical journals and conference proceedings. His present research interests include direct torque control of induction motors, brushless motors, matrix converters, and power quality.

Dr. Casadei is a member of the IEEE Industrial Electronics and IEEE Power Electronics Societies and the Italian Electrotechnical and Electronic Association (AEI). Since 1994, he has been a member of the international editorial board of the international journal *Electromotion*. He is a Registered Professional Engineer in Italy.

Giovanni Serra (A'01) was born in Bologna, Italy, in 1950. He received the Ph.D. degree (with honors) in electrical engineering from the University of Bologna, Bologna, Italy, in 1975.

Following service in the Italian Army, he joined the Department of Electrical Engineering, University of Bologna, first as a recipient of a Fellowship of the Consiglio Nazionale delle Ricerche, then as a Research Associate, and, since 1987, as an Associate Professor. He is currently Professor of Electrical Machines in the Department of Electrical Engineering. He has authored more than 90 papers published in technical journals and conference proceedings. His fields of interests are electrical machines, electrical drives, and power electronic converters. His current activities include direct torque control of ac machines, linear motors, and ac/ac matrix converters.

Dr. Serra is a member of the IEEE Industry Applications and IEEE Dielectrics and Electrical Insulation Societies and the Italian Electrotechnical and Electronic Association (AEI). He is a Registered Professional Engineer in Italy.

Angelo Tani was born in Faenza, Italy, in 1963. He received the "Laurea" degree, with honors, in electrical engineering from the University of Bologna, Bologna, Italy, in 1988.

He joined the Department of Electrical Engineering, University of Bologna, in 1990, where he is currently an Associate Professor. His scientific work is related to electrical machines and drives, power electronics, and Maglevs. He has authored more than 60 papers published in technical journals and conference proceedings. His current activities include ac/ac matrix converters and direct torque control of induction motors.

Luca Zarri was born in Bologna, Italy, in 1972. He received the electrical engineering degree, with honors, from the University of Bologna, Bologna, Italy, in 1998.

He was a Plant Designer with a civil engineering company until 2002. In 2003, he joined the Department of Electrical Engineering, University of Bologna, with which he has been collaborating since 1998. His scientific work is related to electrical drives and power electronics. His research interests include ac/ac matrix converters and direct torque control of induction motors.

Mr. Zarri is a Registered Professional Engineer in Italy.